The evolution of the Sciara del Fuoco subaerial slope during the 2007 Stromboli eruption: Relation between deformation processes and effusive activity

M. Marsella [a],[*], C. Proietti [b], A. Sonnessa [a], M. Coltelli [b], P. Tommasi [c], E. Bernardo [a]

[a] DITS - La Sapienza Università di Roma, Via Eudossiana 18, 00184, Rome, Italy
[b] Istituto Nazionale di Geofisica e Vulcanologia, Catania, Italy
[c] CNR-IGAG c/o Università di Roma, Rome, Italy

ABSTRACT

Focusing on the Island of Stromboli, this research investigates whether airborne remote sensing systems, such as those based on digital photogrammetry and laser scanner sensors, can be adopted to monitor slope deformation and lava emplacement processes in active volcanic areas. Thanks to the capability of extracting accurate topographic data and working on flexible time schedules, these methods can be used to constrain the regular and more frequent measurements derived from satellite observations. This work is dedicated to the monitoring of Stromboli's volcanic edifice which is beneficial when obtaining quantitative data on the geometry of deformation features and the displaced (failures and landslides) and emplaced (lava flows) volumes. In particular, we focus on the capability of extracting average effusion rates from volume measurements that can be used to validate or integrate satellite-derived estimates.

Since 2001, a number of airborne remote sensing surveys, namely Digital Photogrammetry (DP) and Airborne Laser Scanning (ALS), have been carried out on Stromboli's volcano to obtain high resolution Digital Elevation Models (DEM) and orthophotos with sub-meter spatial resolution and a time schedule suitable for monitoring the morphological evolution of the surface during the quiescent phases. During the last two effusive eruptions (2002–2003 and 2007) the surface modifications, created on the Sciara del Fuoco slope and on the crater area as a consequence of effusive activity, were quantified and monitored using the same methodologies. This work, which is based on the results obtained from the multi-temporal quantitative analysis of the data collected from 2001 to 2007, mainly focuses on the 2007 eruption but also accounts for analogies and differences regarding the 2002–2003 event. The 2007 eruption on the Sciara del Fuoco slope from 27 February until 2 April, produced a compound lava field including a lava delta on the shoreline, discharging most of the lava into the sea. The comparison of the 2007 DEMs with a pre-eruption surface (2006 LIDAR survey) allowed for the evaluation of the total lava volume that accumulated on the subaerial slope while two syn-eruption DEMs were used to calculate the average effusion rates during the eruption. Since the evolution of a lava field produced during an eruption can be seen as a proxy for the magma intrusion mechanism, hypotheses are formulated on the connection between the lava discharge and the instabilities suffered by the slope.

© 2009 Elsevier B.V. All rights reserved.

1. Introduction

The recent history of Stromboli's volcano showed that major effusive eruptions can be accompanied by large deformations along the Sciara del Fuoco (SdF) slope. As a matter of fact, the slope can be affected by both wide landslides with tsunamogenic potential, such as those observed in 2002–2003 (Tommasi et al., 2003, 2005; Maramai et al., 2005), or that presumably connected to the 1930 eruption (Rittmann, 1931) and also by large deformations which were not followed by any destructive movement, such as those observed in 2007.

On- and off-shore investigations for analysing morphological features related to recent volcanic activity have been performed on

Stromboli Island since 2001. Surveying activity intensified during the 2002–2003 eruption and was then regularly performed to assess and monitor potential instability phenomena (Puglisi et al., 2005; Baldi et al., 2005, 2008a,b). The surveys carried out between 2006 and 2007 were dedicated to the observation of the 2007 eruption.

The analysis presented here is focused on reconstructing the geometry of the instability phenomenon and its relationship to the effusive activity of the 2007 eruption. In order to conduct this investigation, Digital Elevation Models (DEMs), with an accuracy range of between 0.2 and 0.5 m, were extracted from the data collected by AP and ALS surveys (Table 1). AP surveys also provided images to generate digital orthophotos at a scale greater than 1:5000 (pixel size ranging from 0.5 to 1 m). Aerial data was integrated with orthorectified oblique aerial images (Table 1) taken during daily helicopter surveys by the Italian Department for Civil Protection (DCP). This approach, based on

* Corresponding author. Tel.: +39 44585098; fax: +39 06 44585515.
E-mail address: maria.marsella@uniroma1.it (M. Marsella).

the use of a scientific software specific to the orthorectification of oblique aerial images, increased the quantity of the available georeferenced information (vent and fracture locations, lava field extension, etc.). A multi-temporal analysis of the DEMs allowed for the evaluation of the height variations that were connected to the 2007 eruptive phenomena, i.e. the large deformations that affected the upper portion of the SdF slope and the lava flows emplaced on the subaerial portion of the slope, including the large lava delta built up along the coastline.
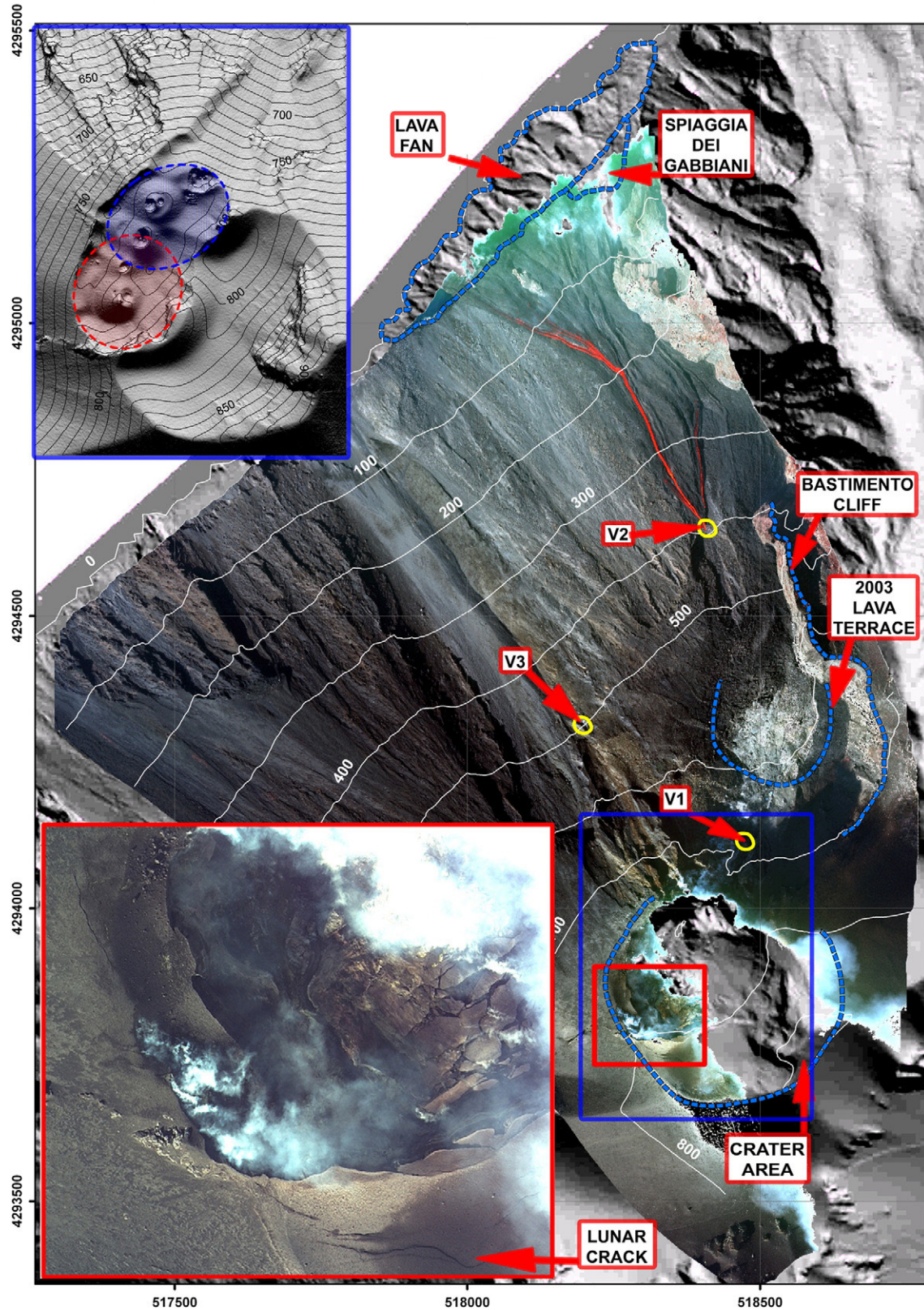
Fig. 1. Orthophoto of 15 March 2007 showing the Sciara del Fuoco slope during the eruption. The background image is a shaded relief view of the pre-eruption DEM. The inset in the top left corner indicates approximately, on the 2006 topography, the North (blue highest ellipse) and South (red lowest ellipse) craters and the vents roughly aligned along a SW–NE direction (azimuth of about 25°). The inset in the bottom left corner shows a magnification of the crater area. (For the colour version of this figure the reader is referred to the web version of this article.)

Table 1
Available data for monitoring the topographic evolution of the SdF and the crater area of Stromboli during the 2007 eruption.

|	Survey data	Aerial platform	Ground coverage	Data acquisition system	Data processing	DEM grid size (m)	Orthophoto pixel size (m)
Pre	22/07/2006	Nuova Avioriprese S.r.l.	Island	Optech ALS ALTM 3100 100 kHz	Microstation suite Terrascan	1–5	–
Syn	04/03/2007	Centro Informazioni Geotopografiche Aeronautiche	SdF	AP camera Wild RC20	Digital Photogrammetric Workstation SOCET SET v5.4.0		1
	04/03/2007	DPC - Helicopter	SdF	Calibrated digital camera Nikon D100	OrthoView v1.3	–	0.3
	15–16/03/2007	Nuova Avioriprese S.r.l.	SdF	Digital mapping camera Z/I Imaging DMC®	Digital Photogrammetric Workstation SOCET SET v5.4.0	1–5	0.5–1
	28/03/2007	DPC - Helicopter	F2 lava flow	Calibrated digital camera Nikon D100	OrthoView v1.3	–	0.5
Post	12/04/2007	Nuova Avioriprese S.r.l.	SdF	AP camera Wild RC20	Digital Photogrammetric Workstation SOCET SET v5.4.0	1–5	0.5
	22/05/2007	Nuova Avioriprese S.r.l.	Island	Optech ALS ALTM 3100 50 kHz	Microstation suite Terrascan	1	-

The collected data was used by the scientific community during the emergency phase to support the DCP's decisions. Furthermore, the obtained results, reinforced by the comparison with those related to the 2002–2003 event, helped to improve the knowledge of the connection between the magma extrusion and instabilities of the SdF slope. This data, which quantitatively describes syn-eruption instability scenarios, represents a starting point from which to carry out research and investigations on risk assessment for the Stromboli volcano.

2. Eruption history

At the onset of the 2007 Stromboli eruption, a large rockfall occurred (27 February, 12:39 GMT), thus anticipating the opening (12:48) of the V1 vent at 650 m a.s.l. (Fig. 1) on the north–east flank of the North crater (Cristaldi, 2007). Lava outpoured from this vent spread on the lava terrace that had formed during the 2002–2003 eruption, thus forming two distinct flow branches (F1a and F1b, Fig. 2) that propagated to the steep SdF slope and then rapidly reached the sea. The northern branch

(F1a) propagated along the base of the Bastimento cliff forming a fan of about 60 m in width on the Spiaggia dei Gabbiani, while F1b was emplaced on the central portion of the SdF, covering the 2002–2003 lava field (Marsella et al., 2008).

A few hours after the eruption's onset, a marked increase in seismic signals was recorded at 17:06 by the Istituto Nazionale di Geofisica e Vulcanologia (INGV) seismic network (Patanè, personal communication) and heralded a large gravitational movement involving the SdF slope: the lava terrace experienced a substantial vertical movement whereas a bulging of the slope was observed at a lower elevation (Fig. 3a). At 18:29 the main eruptive vent V2 (Fig. 1) opened at the front of the displaced mass (at about 400 m a.s.l) as evidenced by a small hot-rock avalanche which was recorded by the Civil Protection surveillance camera. While the V1 vent became inactive, the newly formed F2 flow (Fig. 2) rapidly reached the sea where it partly overlapped and enlarged the F1a lava fan toward the Spiaggia dei Gabbiani. Between 28 February and 4 March 2007 the F2 flow was characterized by several overlapping flow units which
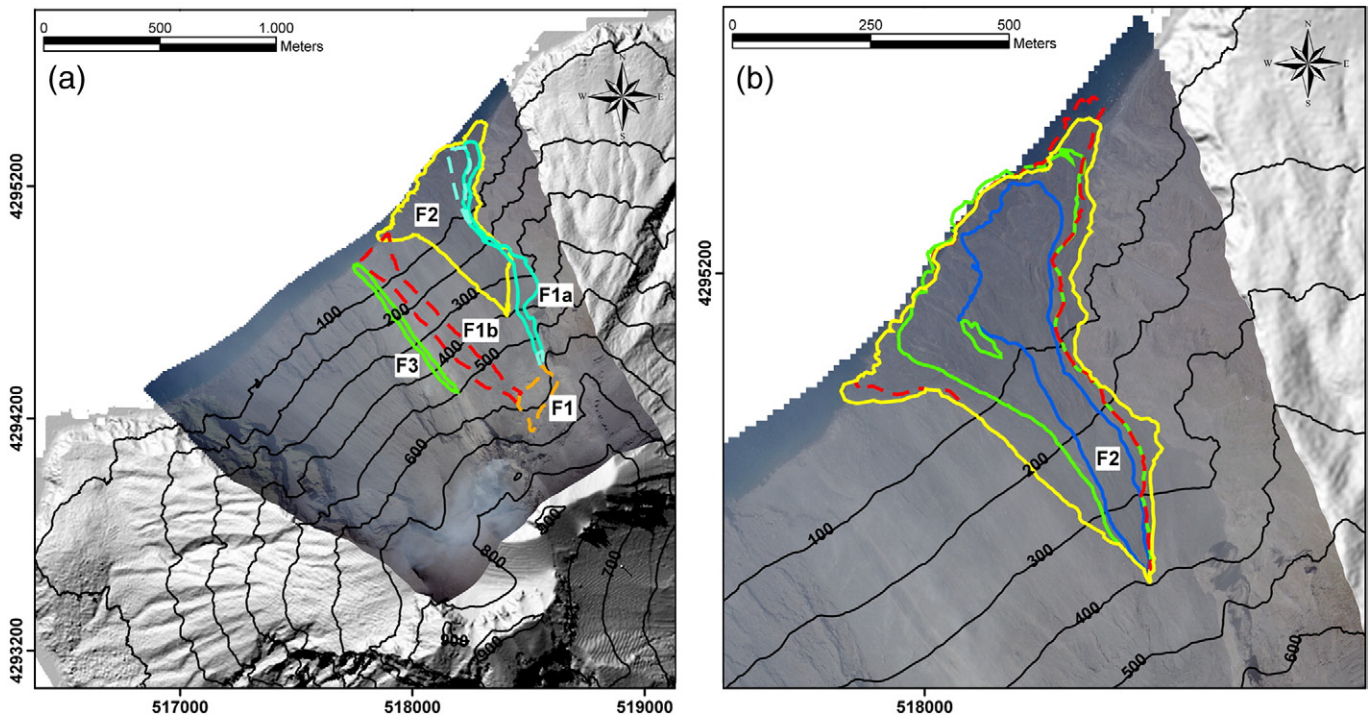
Fig. 2. (a) Lava field produced during the 2007 eruption. Dashed lines limit flows or portions of them that cannot be identified on the orthophotos. Contour lines from the 22 May 2007 ALS survey are drown every 100 m. (b) Evolution of the F2 flow at 4 March (blue line), 15–16 March (green line), 28 March (red dashed line) and 2 April (yellow line). In a) and in b) the background images are the post-eruption orthophoto (12 April) and the pre-eruption shaded relief (2006). (In the printed version see the legend in figure b for reference to the colour; for the colour version of this figure the reader is referred to the web version of this article.)
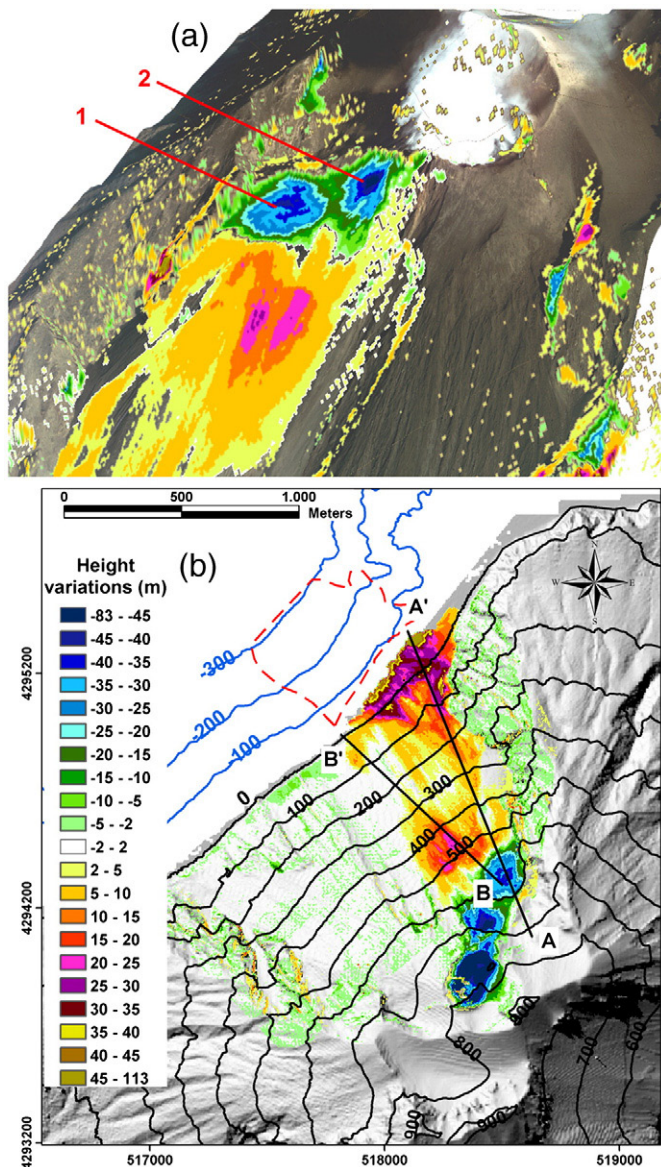
Fig. 3. (a) 3D view of the upper portion of the Sciara del Fuoco with superimposed the residual map (same color scale as in b) showing the height variation at the end of the eruption and highlighting the lowering (up to about 50 m) of the lava terrace (1) and the instability at the base of the North Crater (2) and the bulging (yellow to violet, up to 30 m) in the medium sector of the slope; (b) map of the residuals between the 2007 and 2006 DEMs; black contour lines every 100 m are extracted from 2007 DEM; the shoreline refers to the 2006 survey; blue contour lines (grey in the printed version) are drown every 100 m from a pre-eruption bathymetric survey (Baldi et al., 2008b); the black straight lines define the sections shown in Fig. 4. (For the colour version of this figure the reader is referred to the web version of this article.)

feeding three small emptying flows. On 9 March (at roughly 15:00), soon after the short V2 interruption, a new vent (V3, Fig. 1) opened at 500 m a.s.l. feeding the F3 lava flow which reached the sea in less than three hours and lasted approximately one day. The F2 flow was again fed from 9 March at about 04:00 and once more produced several overlapping flow units, some of which reached the sea. The F2 lava fan widened and completely overlapped that of the F1a flow (Fig. 2b) to about 480 m and its outspreading, compared to the pre-eruption coastline, ranged from 60 to 150 m.

On 15 March 2007 at 20:37 an explosive paroxysmal event occurred at the summit craters with a magnitude and a style similar to that of 5 April 2003 (Ripepe et al., 2005; Rosi et al., 2006): it started as an ash-cloud emission and then evolved into a column-forming eruption that produced a wide fallout of lapilli and spatters reaching Ginostra, and large blocks ejected toward Stromboli village (Andronico et al., 2007).

The V2 vent fed one to three lava branches between 19 and 24 March. The lava channels experienced local tunnel formations and an increased bifurcation process near the shoreline, favouring the lava fan expansion. The lava flow field was again mapped on 28 March using an orthorectified image taken from a helicopter and on an aerial orthophoto from the 12 April (Fig. 2b). On the basis of both images, the portion of the lava delta protruding from the sea measured about 670 m wide and outspread between 40 and 120 m (less than the length measured on 16 March due to a bench collapse) from the pre-eruption coastline. A lava delta this large had not been seen at Stromboli since the 1955 eruption.
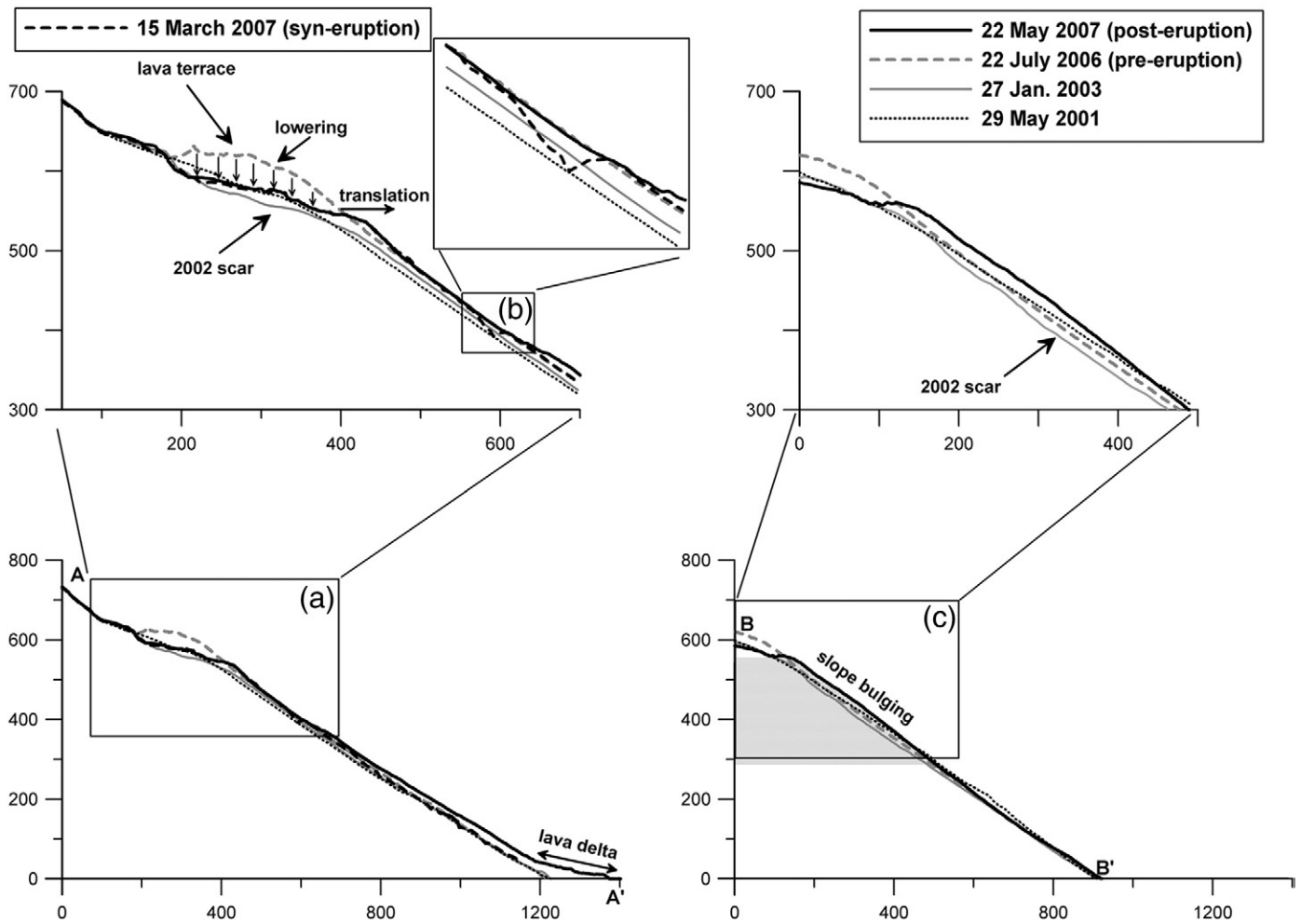
The discharge from the main vent (V2) ended on the evening of 2 April 2007, leaving a compound fan-shaped flow field on SdF which also extended significantly along the underwater slope.

3. A geometric reconstruction of the slope failures

The deformations that affected the SdF slope can be visualized through a 3D view of the upper portion of the SdF, onto which the height variations (residuals) observed at the end of the eruption are superimposed (Fig. 3a). The analysis of the residual map between the pre- and post-eruption DEMs (Fig. 3b) allows us to display the magnitude and spatial distribution of the deformations suffered by the slope, where they were not hidden by the subsequent lava flows and by the landslide debris. In particular, Fig. 3 highlights the lowering of the 2003 lava terrace (up to about 50 m), the failures in the North crater's north-eastern wall (about 0.84×10^6 m^3) and the bulging in the medium sector of the slope (between about 550 and 350 m a.s.l.). The latter effect, which appears on the residual map as an uplift up to 30 m which gradually decreasing downwards, can only be explained as having been induced by a large horizontal displacement. This is evidenced in Fig. 4 which shows the longitudinal profiles of the slope. The profiles outline the slope before and after the 30 December 2002 landslide (29 May 2001 and 27 January 2003 respectively), and clearly show the lava terrace that formed during the 2002–2003 eruption (22 July 2006) and its lowering at the onset of the 2007 eruption (15 March 2007). Section AA' evidences the translational component which accompanied the lowering of the terrace and intersects the scar left by the 27 February 2007 movement just above the V2 vent, which was later filled in during the eruption. Section BB' illustrates the way in which the scar left by the 30 December 2002 landslide was filled by the lava outpoured during the 2002–2003 eruption, almost recreating the pre-eruption shape, before being bulged in the first phase of the 2007 eruption.

3.1. The lowering of the lava terrace

The analysis of oblique aerial syn-eruption photos, the post-eruption orthophoto and the DEM allows us to identify and map some key elements which are useful when quantifying the mass displaced by the failure phenomena at the slope top and when attempting to reconstruct the kinematics of the movement. The mechanism of the

reached the sea, thus widening the lava fan to about 180 m and spreading it over 90–100 m.

Between 5 and 6 March several arcuate tension cracks (lunar cracks) were observed on the South crater's southern sector (Fig. 1) initiating a rapidly evolving instability which propagated northward in a matter of days, causing the extensive collapses that were observed by the INGV surveillance cameras on 10 March. Subsequently, the internal walls of the crater depression exhibited a wide variety of degradational states, including slumps and falls, best observed in the south-eastern section where lunar cracks continued to expand causing progressive mass wasting until the end of the eruption.

The F2 flow was sustained continuously until the afternoon of 8 March when a short interruption caused the cooling of the lava flow front and, further uphill, the formation of two ephemeral vents

Fig. 4. Longitudinal sections AA' and BB' (Fig. 3b) show the modifications of the Sciara del Fuoco slope between 2001 and 2007, namely at 29 May 2001, 27 January 2003 (after the 30 December 2002 landslide), 22 July 2006 (after the 2002–2003 and before the 2007 eruption), 15 March 2007 (AA' only, during the 2007 eruption and after the slope movement) and at 22 May 2007 (after the 2007 eruption). The insets highlight (a) the 2002–2003 lava terrace, (b) the scar left by the 27 February 2007 movement just above the V2 vent and (c) the slope bulging.

main failure phenomena, which involved the 2002–2003 lava terrace, can be reconstructed by observing structural and morphological features visible on the post-eruption shaded relief map when compared to the pre-eruption one (Fig. 5).

As with the beginning of the 2002–2003 eruption, the main failure occurred downhill of the dike which is assumed to feed the eruption. Fig. 5a shows the trace of the dike which intersects the summit vents, the 2007 eruptive fissure and the first vent (V1), aligned almost along the same trend as the 2002–2003 main vents (Fig. 5b).

Fig. 6 illustrates some useful key elements in understanding the geometry of the main displaced body, which is roughly delimited by the blue arrows in Fig. 6a. The outcropping traces of the disconti-nuities which mark the movement are indicated by dashed lines (Fig. 6a). It is most likely that the main scarp (1) of the failure surface follows the contact between the SdF infilling deposit and the substratum and extends from the foot of the Bastimento cliff up to the northern base of the crater area, just below the large breach which opened at the onset of the eruption. The scarp is steep with a vertical throw of more than 30 m. The NE side (2) seems to develop parallel to the Bastimento, while the SW side (3) can be identified by the alignment of a series of small persistent fractures located at the base of the crater. The trace of the basal surface (4) can be identified by an elongated area of loose material also evidenced by a step, extending from the Bastimento wall along a SW–NE alignment.

The volume of the displaced mass involved in the failure can be evaluated using the simplified geometry of a wedge-shaped body with

six faces. They corresponds to the topographic surface at the top and the front, and to the surface which was uncovered by the lowering of the lava terrace, at the back. This represents the main scarp (line 1, in Fig. 6a) and runs from the base of the crater area to that of the Bastimento cliff. Further uncertainties remain for the positioning of the bottom surface (line 4, in Fig. 6a) and the extension of the lateral ones (lines 2 and 3, in Fig. 6a).

If we adopt this schematic description, two different displaced volume estimates can be obtained: about 5×10^6 m³, evaluated by assuming that the wedge extends downwards to the fractured area above the V3 vent and the trace of the basal surface (green in Fig. 6b) identified as described above; about 8×10^6 m³, evaluated by assuming that the wedge extends down to the central zone of the bulging area, where the basal surface (red in Fig. 6b) is presumed to extrude, and it is delimited on the western side by a surface reaching the V3 vent.

3.2. Crater area collapse

As a consequence of the slope failure and the effusive activity, the crater area underwent relevant morphological changes. The deforma-tion process that affected the north-eastern sector of the SdF slope modified the state of stress in the neighbouring areas, and particularly within the crater area which fractured and suffered the formation of a large breach along the north-eastern rim of the North crater. This failure can be related to the lowering of the lava terrace which undermined the crater flanks already weakened by the 2002–2003
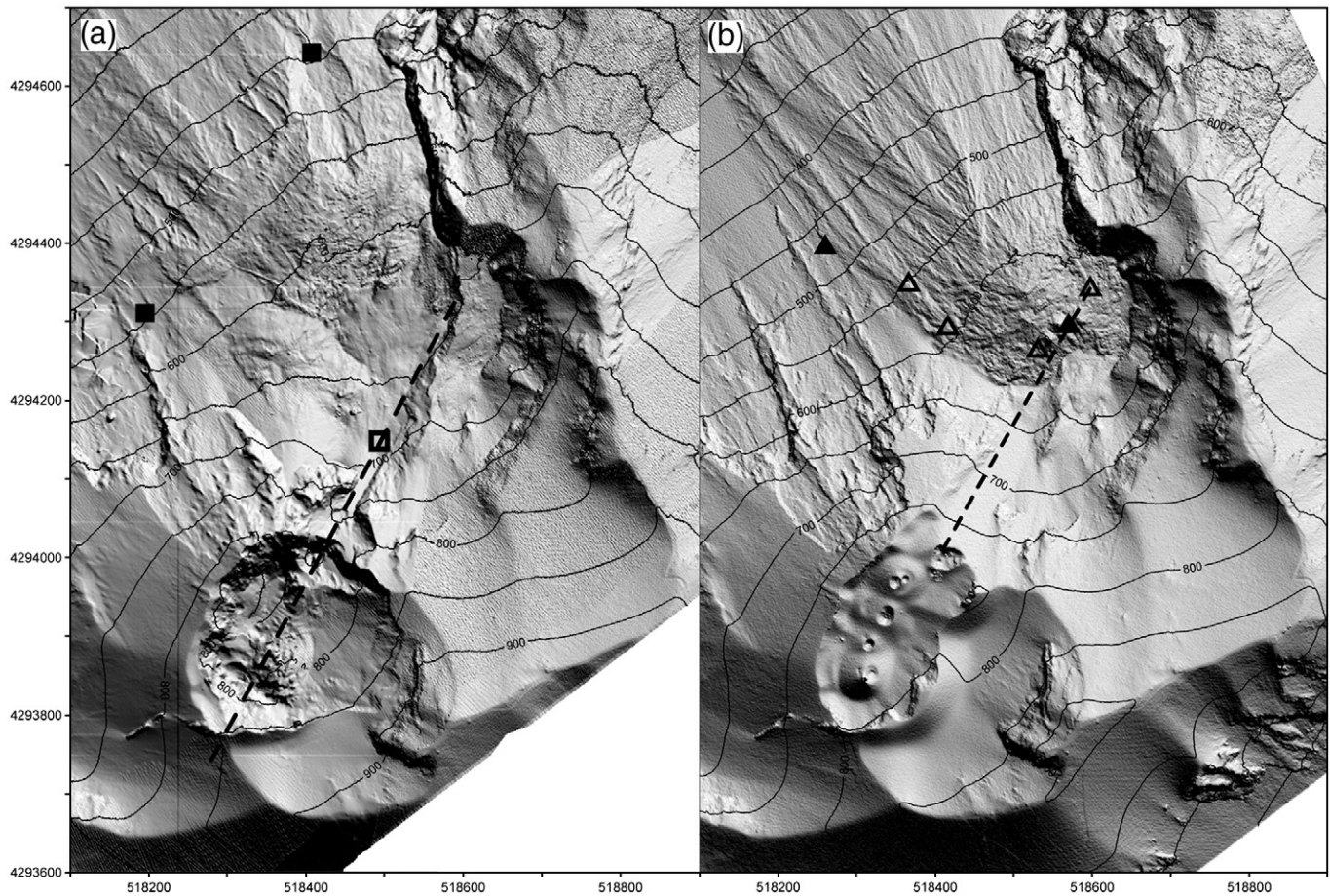
Fig. 5. (a) Shaded relief and contour lines drawn every 50 m of the post-eruption DEM (May 2007), squares locate the vents of the 2007 eruption; (b) Shaded relief and contour lines drawn every 50 m of the pre-eruption DEM (July 2006), triangles indicate the main vents of the 2002–2003 eruption. On both images, vents represented as filled symbols were measured on the orthophotos, whereas the empty ones were located through the analysis of helicopter photos and eyewitness reports; dashed lines indicate the traces of the dikes.

eruption. On the contrary, it is not possible to establish a straightforward relationship between the changes in the state of stress induced by the slope movement and the failures characterising the inner sector of the south-eastern zone of the crater area.

These processes should be directly related to the emptying of the magma reservoir during an advanced phase of eruption. As a matter of fact, these failures started at the south–west as testified by the lunar cracks visible since the beginning of March (Fig. 1). Then the portions comprised between the fractures and the crater rims gradually moved towards the crater interior and the fractures also extended to the north-eastern sector of the crater (Fig. 7a).

The volume involved in the collapses on the south-eastern sectors of the crater area was estimated assuming, for the slip surface of the unstable body, a semi parabolic or planar shape. The area affected by the failure was delimited on orthorectified helicopter images (Fig. 7a), while five sections were cut radially to the crater area (Fig. 7b) on the pre-eruption DEM (ALS 2006). This allowed us to calculate the volume by subdividing the body into different slices with varying geometry. The volumes of each portion were then evaluated by multiplying the average area of the two transversal sections, delimiting it by their average distance. The estimated volumes were 1.13×10^6 m^3 and 1.55×10^6 m^3 for the wedge
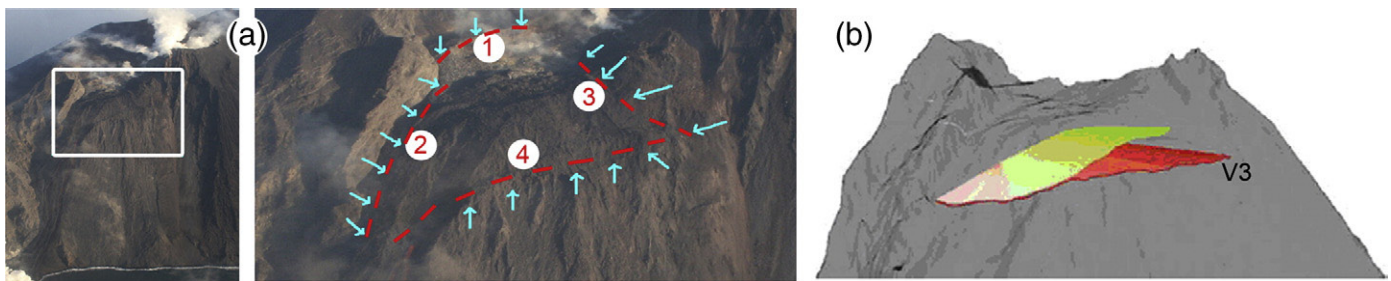
Fig. 6. (a) A frontal view of the Sciara del Fuoco slope, where the white rectangle delimits the area in the right figure and the dashed lines identify the outcropping traces of the discontinuities which mark the movements; (b) 3D shaded relief of the same area showing the two possible locations of the basal surface: green (the lightest in the printed version) or red (the darkest in the printed version). (For the colour version of this figure the reader is referred to the web version of this article.)
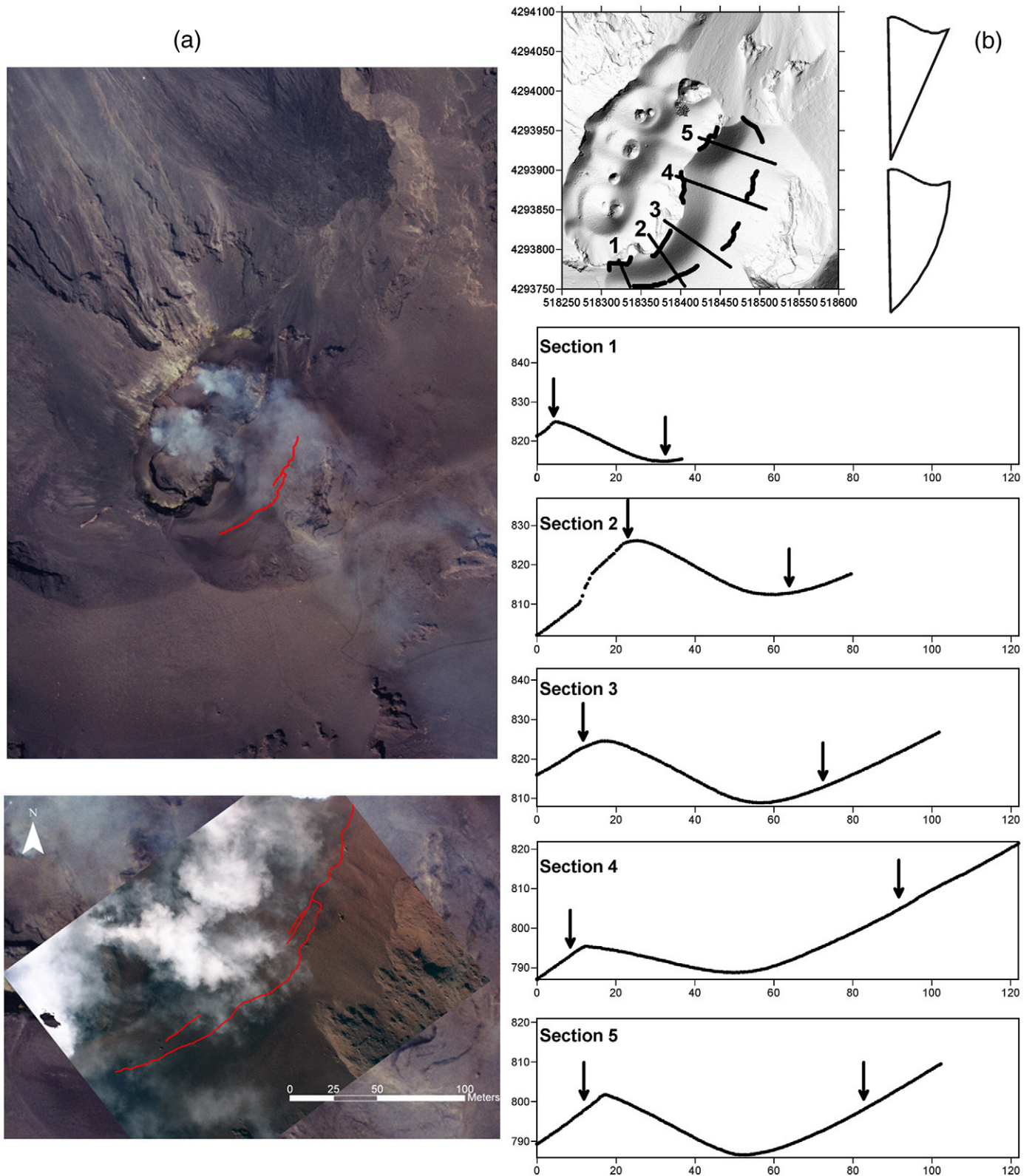
Fig. 7. (a) Syn-eruption orthophotos of the crater area used to delimit the area affected by failures; (b) Shaded relief (2006 DEM) of the crater area, where black lines indicate the traces of the five radial sections shown below and the dashed black line delimits the unstable zone of the south-east sector of the crater area. Wedge or semi-parabolic shapes (on the right) have been adopted to quantify the unstable body. Sections 1 to 5 cut on the 2006 DEM: the x-axis represents the progressive distance (meters) and the y-axis the height a.s.l.; black arrows indicate the intersection between each section and the unstable area's external limit. (For the colour version of this figure the reader is referred to the web version of this article.)

and parabolic-shaped sections respectively. The comparison between the 2007 and 2006 ALS DEMs (Fig. 5) provided a value of circa $1.64 \times 10^6 \, \text{m}^3$ for the total mass that had collapsed inside the craters from the surrounding area.

4. Evaluation of the lava flow volumes and effusion rate

A multi-temporal analysis of the collected data allowed us to define the final geometry of all of the lava flows and to monitor the

Table 2
Total area, total volume and average thickness of the F1, F1a, F1b and F3 flows (volume evaluated by the planimetric approach).

Lava flow	Effusion start	Effusion end	Total area (10^6 m^2)	Average thickness (m)	Total volume (10^6 m^3)
F1	27/02 14:00	27/02 19:30	0.02	5.5	0.11
F1a	27/02 14:00	27/02 19:30	0.05	6.0	0.30
F1b	27/02 14:00	27/02 19:30	0.07	3.0	0.21
F3	09/03	10/03	0.02	1.5	0.03

evolution of the F2 lava flow, the only one that remained active throughout the whole eruption.

The flow volumes were evaluated by comparisons between syn, post- and pre-eruption DEMs (Table 1), together with an orthophoto analysis to delimit the lava flows (Fig. 2). Nevertheless, some problems arose when defining the flow geometry, owing to the relevant morphological modifications which occurred at the onset of the 2007 eruption that then made the 2006 DEM unsuitable as a reference surface for lava volume estimation.

Both the planimetric (area by average thickness) and topographic (difference between post- and pre-eruption DEMs) approaches (Stevens et al., 1999; Coltelli et al., 2007) were adopted to evaluate the lava flow volumes. Final volumes (Table 2) were assessed for short-lived flows (F1, F1a, F1b and F3) whereas cumulative subaerial volumes were evaluated throughout the long-term emplacement of the F2 flow (Table 3).

The planimetric approach was adopted for the flows (F1, F1a, F1b and F3) emplaced on areas where deformations at the beginning of the eruption induced displacements that exceeded the lava thicknesses (Table 2). In particular, F1 and the upper portion of F1a were emplaced on the lava terrace (Baldi et al., 2005) which underwent a downfall as great as 50 m, while the lower portion of F1a was partially buried by F2. F1b coincided with the bulging area that suffered an uplift of about 30 m, and most of the emplaced volume of F3 — a sheet lava flow — was rapidly removed before it could be quantified.

The volume of the subaerial portion of F2 (Table 3) was evaluated by integrating the planimetric and topographic approaches (see Appendix A) because it was emplaced on an area affected by a landslide preceding the lava emission. The landslide's extension was defined by analysing the residual map at 4 March (Fig. 8) where negative residuals have been associated to the intersection between the lava flow and the landslide. Most of the lava emitted by the F2 vent reached the sea where it built a wide lava delta leaning on the submarine SdF slope which partially overlapped and expanded the one emplaced by the F1a flow.

The secondary vents (V1 and V3) emitted about 0.65×10^6 m^3 (Table 2), although this value has been slightly underestimated because the F1a flow had built a small lava fan that was then buried by the F2 delta. The final volume emplaced on the subaerial slope by the main vent (V2) was 2.70×10^6 m^3 (Table 3).
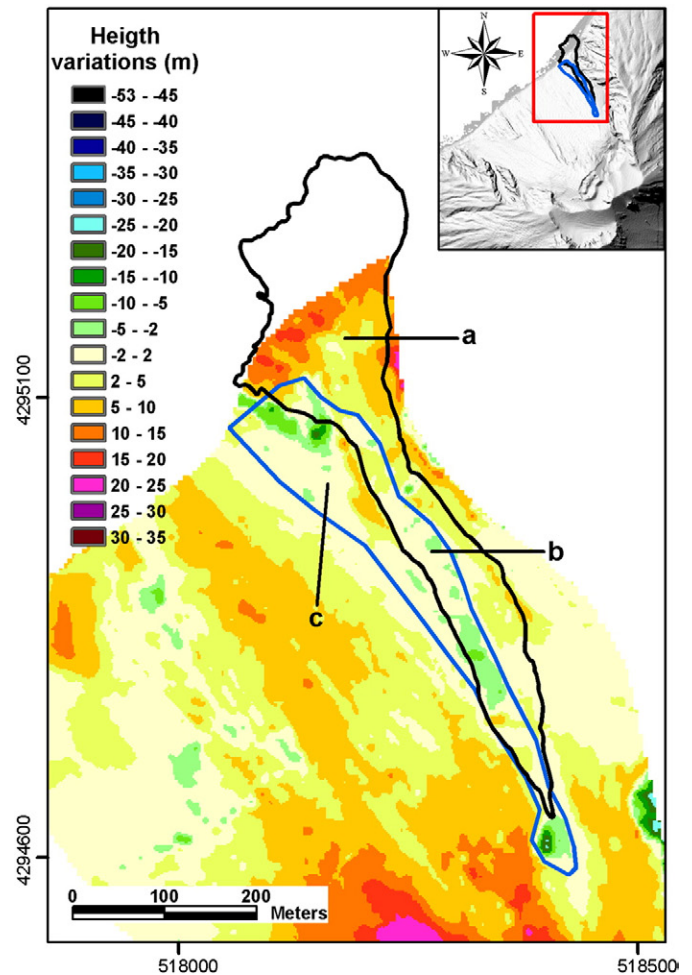
The final lava volume deposited below sea level (Table 4) was estimated by differentiating two surfaces: the upper one corresponding to the submarine lava bench which was reconstructed, accounting for a typical lava deposition angle along a submarine slope (Moore et al., 1973), and the lower one being obtained from the pre-eruption bathymetry (Baldi et al., 2008b). The estimated final volume was used

Fig. 8. F2 lava flow and landslide limits defined above the residual between the 4 March 2007 and 22 July 2006 DEMs, evidencing the three areas used for evaluating the filled and removed volumes respectively covering (a) the whole F2 flow, (b) the intersection between F2 and the landslide, and (c) the landslide outwith the F2 limit. (For the colour version of this figure the reader is referred to the web version of this article.)

as a constraint for extrapolating backward the partial volumes at the dates on which subaerial slope volumes were calculated (Table 4). Adding the total lava emplaced on the subaerial to that estimated for the submarine portion a volume of 10.86×10^6 m^3 is obtained for the lava discharged during the entire 2007 eruption. Partial volumes in two subsequent surveys were divided by the corresponding time span thus providing the average effusion rate (Table 4).

In Fig. 9, cumulative volumes and average effusion rates, estimated for the 2007 eruption as described above, are compared to those obtained during the 2002–2003 eruption in order to highlight that

Table 3
Temporal evolution of total area and volume and average thickness of the F2 flow on the subaerial slope (volume evaluated by integrating the planimetric and topographic approaches).

Survey date	Total area (10^6 m^2)	Average thickness (m)	Total volume (10^6 m^3)
04/03	0.06	3.1	0.20
15–16/03	0.13	11.0	1.44
12/04*	0.18	15.0	2.70

*The corresponding values refer to the end of the eruption (2 April).

Table 4
The total subaerial volume is the sum of the volumes of the five lava flows; the submarine volume is related to F1a and F2 flows; the total emitted volume is the sum of the total subaerial and submarine volumes; the partial volume is the difference between the total emitted volumes in two subsequent surveys; the time span is the temporal interval between two subsequent surveys and the average effusion rate is the partial volume divided per time span.

Survey date	Total subaerial volume (10^6 m^3)	Submarine volume (10^6 m^3)	Total emitted volume (10^6 m^3)	Partial volume (10^6 m^3)	Time span (d)	Average effusion rate (m^3/s)
04/03	1.05	2.40	3.45	3.45	5	7.98
15–16/03	2.09	4.71	6.79	3.34	12	3.22
12/04*	3.35	7.51	10.86	4.07	17	2.77

*The corresponding values refer to the end of the eruption (2 April).
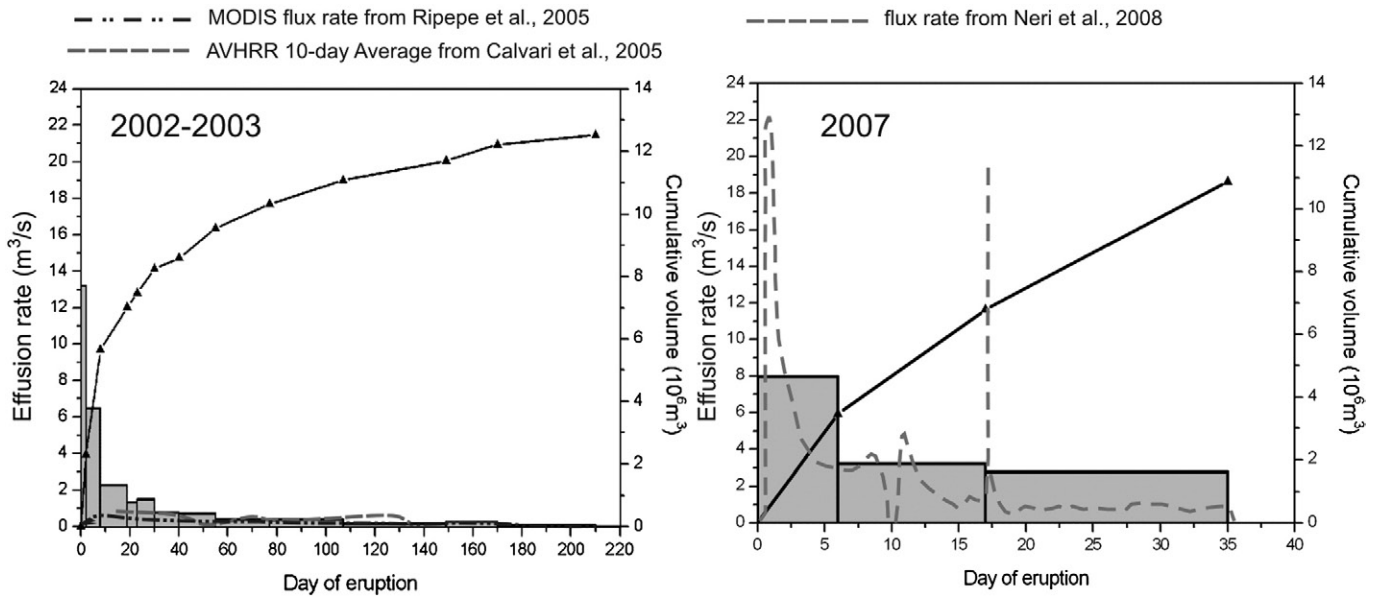
Fig. 9. Temporal evolution of average effusion rates (filled grey bars), and cumulative volumes measured from aerial surveys (black lines and triangles); satellite effusion rates are also redrawn from Calvari et al. (2005); Ripepe et al. (2005) and Neri et al. (2008). Data in (a) refers to the 2002–2003 eruption, while that in (b) to the 2007.

dike intrusions within the SdF slope can result in different eruptive behaviours. The 2002–2003 event was a long-lasting one (210 days) characterised by a peak followed by a quite abrupt exponential decline and then by a longer fading phase until the end of the emission (Marsella et al., 2008). The 2007 eruption went on for only 35 days and appears to have been characterized by a sudden ending rather than by a long phase of moderate emission. Unfortunately, only three syn-eruption aerial surveys were carried out, thus it has not been possible to detect any short term variations of the effusion rate.

Fig. 9 also includes effusion rate trends for the 2002–2003 eruption obtained through the analysis of thermal satellite images reported by Calvari et al. (2005) and Ripepe et al. (2005), and by Neri et al. (2008) for the 2007 eruption. Fig. 9a shows that the three 2002–2003 trends are quite comparable, although the initial peak was undetected (or the data is insufficient) by the satellite surveys. Fig. 9b shows that also the 2007 effusion rate trend presents an initial peak, which is more marked by the satellite data and less noticeable in our average estimate because of the lack of a second aerial survey in very first few days of the eruption. Taking into account our results, the second phase of the eruption is characterized by average effusion rates in the order of 3 m³/s and clearly accounts for the rapid decrease of the lava discharge rate that terminated the eruption. Conversely, satellite data provide effusion rate values systematically lower than that of our average values and depict a situation similar to that observed for the 2002–2003 eruption with a very short fading phase until the end of the emission.

On the basis of the effusion rate trends obtained from the multi-temporal analysis conducted on the two eruptions, several considerations can be outlined to identify different outpouring mechanisms. Therefore, the 2002–2003 eruption can be divided into three phases. Firstly, there was a high discharge from a broken conduit, preceding and probably accelerating the dike intrusion from below, followed by a sudden slope decompression that opened a lateral path for magma emission and accelerated the elastic strain relaxation on the shallow dike. Finally, a longer phase in which the effusion rate was controlled by a strain energy release from the sub-volcanic reservoir was recorded (Marsella et al., 2008). On the other hand, the 2007 eruption can be interpreted as a two-phased event including a peak phase (unfortunately unconfirmed by the available photogrammetric data but inferred from direct observations and satellite data) followed by a short phase (only one month) characterised by moderately stable effusion rates before the eruption was abruptly terminated.

5. Hypothesis on the deformation and fracture mechanism

Regarding the mechanisms that controlled the slope deformations which occurred shortly after the eruption onset, a hypothesis has been put forward on the basis of the deformation pattern. Morphological/structural elements observed on the slope and geotechnical considerations were obtained from numerical models and mechanical tests on the SdF volcaniclastic material.

Stability analyses conducted to understand the failures linked to the 2002–2003 eruption indicate that the slope is stable under purely gravitational stresses; it was also observed that even significant seismic actions, like those produced by the 2003 paroxysmal explosion, had not induced instability phenomena (Tommasi et al., 2005). Values of the shear strength parameter of the SdF infilling material's weakest component, determined through large-scale laboratory tests, turned out to be relatively high so that, by assuming a pure frictional strength, peak friction angles varied in the range of 40–42° (Tommasi et al., 2007). Thus the wedge-shaped portion of the slope (Fig. 6), delimited by a sub-horizontal basal failure surface, does not become unstable even under dynamic loads like those expected during the initial phase of the 2007 eruption. For this reason, the wedge did not detach from the slope even after its large displacement so no rock avalanches occurred. Instead, the movement formed the large shear zone along its southern lateral boundary which undermined the outer flank of the northern crater causing repeated slides.

Some elements suggest that the deformation and failure processes that occurred at the summit of the SdF in the afternoon of 27 February 2007 were initiated by a magma intrusion. As a matter of fact, the large wedge (Fig. 6) is closely linked to the magma paths within the upper part of the slope. Both the intersections between the two lateral limits of the wedge (sides at NE and SW) and the trace of the basal shear plane on the surface are located in proximity to the two eruptive vents V2 and V3 (Fig. 1). Furthermore, the rear of the wedge corresponds to a sharp discontinuity predating the 2007 eruption which was produced by a blade-like intrusion occurring at the onset of the 2002–2003 eruption. As a matter of fact, the 2002–2003 vents (Fig. 5b) should be aligned along the direction of the shallow portion of the magma intrusion and should consequently mark the strike of the eruptive fissure. When the 2007 eruption started, this discontinuity represented a weak zone within the SdF deposit and, consequently, a preferential path for a new magma intrusion.
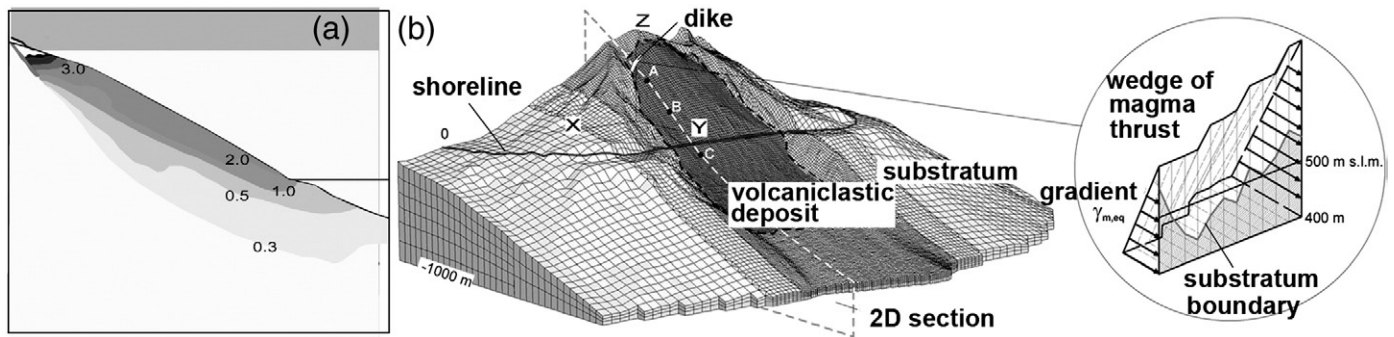
Fig. 10. (a) Contours of horizontal displacements calculated for an intruding blade-like dike; contour lines evidence the formation of a plastic wedge at the slope top; (b) General slope geometry used in the analysis and scheme for the calculated magma forces (circular inset).

Moreover, 3D Finite Difference (FD) analyses performed by Graziani et al. (2007) with the FLAC 3D code, which analysed the 2002–2003 failure phenomena, reinforce to the hypothesis of the triggering action of the magma intrusion. These analyses clearly indicate that, with a slope geometry similar to that existing in 2007, an apparently plastic wedge forms at the slope top as a result of forces exerted by a blade-like magma intrusion (Fig. 10a). The analyses were conducted assuming the magma pressure distribution reported in Fig. 10b (Tommasi et al., 2007) and using the small-strain configuration (Itasca, 2006), i.e. calculations are interrupted when displacements are still relatively small, thus reproducing the initial failure conditions.

However, the deformation pattern derived from aerial data analysis cannot be fully explained by the simple extrusion of a wedge due to a back-thrust. In fact the bulging is not limited to the zone underneath the slope break but extends downwards, and the lowering of the lava terrace (i.e. the wedge top) exceeds the vertical component of the displacement that is usually produced by a dike thrust. Two different mechanisms can thus be proposed: a rapid and intense magma withdrawal within the dike or a double-wedged failure (e.g. Kovari and Fritz, 1984). The former hypothesis was verified through 3D FD analyses which showed a significant displacement that was extremely localised around the dike. The latter mechanism (Fig. 11) would justify both the lowering and disarrangement of the lava terrace and would also account for the extension of the bulging at a lower elevation. As the sliding of the lower part of the displaced mass proceeds, a "sinking" (or sagging) of the slope top, overloaded by the lava mega-tumulus emplaced during the 2002–2003 eruption, develops.

The effectiveness of the upper wedge in inducing deformations on the slope below was enhanced by a reduction of strength along its basal and lateral faces that occurred during the extrusion and was demonstrated by the formation of a frontal fracture behind the slope break, visible in aerial photographs. Deformations gradually decreased, proceeding downslope because of the progressive loss of influence of the dike thrust (Fig. 10a). This effect could have been favoured by the mechanical behaviour of the volcaniclastic material that, excluding low confinement stresses, has a contractive behaviour (Tommasi et al., 2007).

In regard to the intrusion process, the formation of sharp discontinuities could have driven and controlled the outpouring of the magma at a lower elevation: lava emission from V2 can be seen as evidence of the existence of a structural discontinuity at the base of the wedge. Similarly, the short-lived lava emission on 9–10 March 2007 from the V3 vent, at the same period as the brief rest of V2, seems to have occurred at the intersection between the basal and the southern lateral face of the upper wedge.

6. Analogies and differences between the 2002–2003 and 2007 Stromboli eruptions

A comparison of the 2002–2003 and 2007 eruptions provides some interesting suggestions on the interaction between dike intrusion and the stability of the SdF slope.

During the 2002–2003 eruption, the back-thrust exerted by the dike intrusion provoked the failure of a large part of the SdF top and triggered a deep movement which also involved the submarine slope. Extensive deformations also evolved slowly during the first two days, producing large vertical and horizontal displacements. Such instability phenomena involved a deposit that had not been disarranged by recent movements. The main consequences of the eruption were a wide landslide on the SdF central portion and a buildup of a thick lava terrace at the slope top at the base of the Bastimento cliff.

During the 2007 eruption, the slope was again interested by the failures of the summit portion of the SdF although instabilities were relatively shallow and were limited to the upper third of the subaerial SdF, whereas the lower sector was slightly modified. Moreover, the most significant movement occurred over a few hours. The instabilities of the 2007 eruption affected an area of the slope which had been significantly weakened by the 2002–2003 slides. The same area was then overloaded at the top by a 50-meter thick lava pile and partly covered at a lower elevation by debris and lava flows which were deposited over a short time span. The main consequences of the 2007 eruption can be identified in the lowering of the 2002–2003 lava
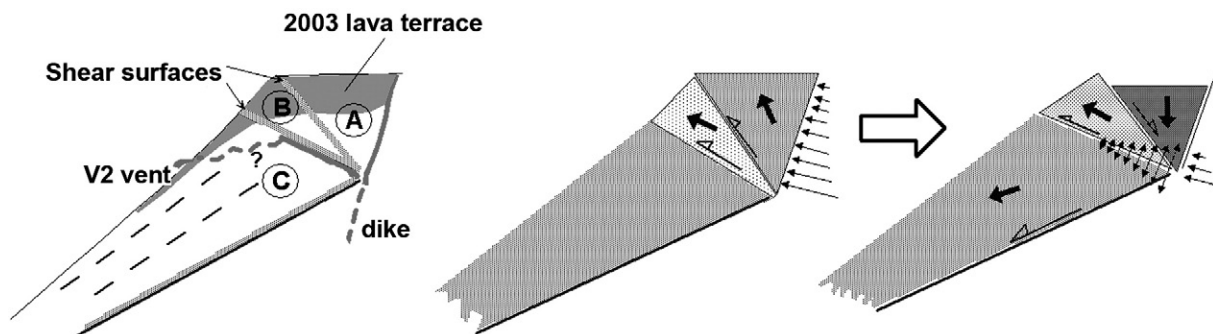
Fig. 11. Sketch of the kinematics of the wedge-shaped body; dashed lines in the left part of the figure resemble the infilling deposit; the thinnest arrows, in the central and right parts of the figure, indicate the acting forces, while the bold arrows and those with the empty head indicate the displacement directions.
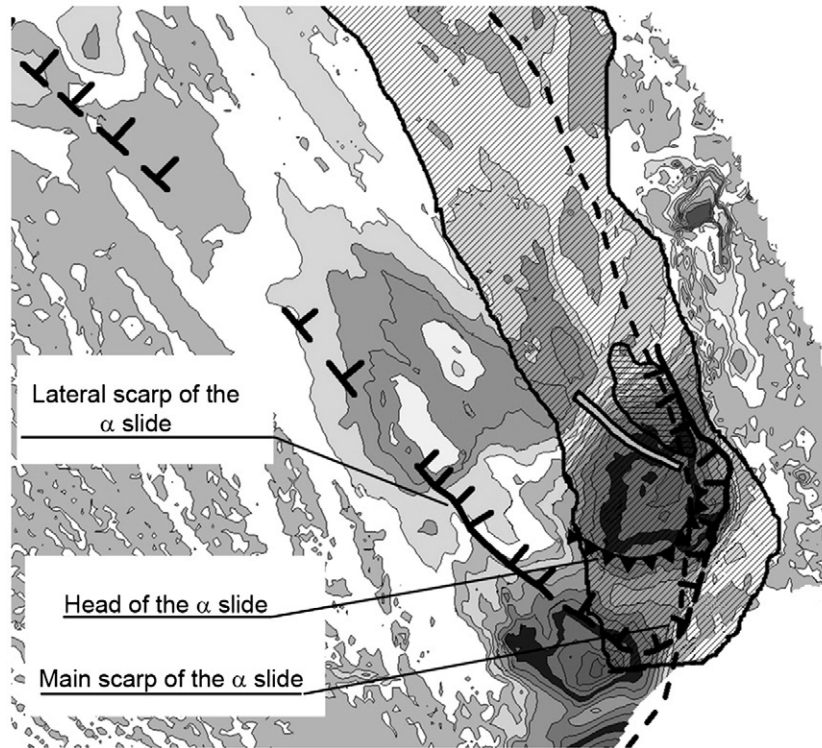
Fig. 12. Final residual map of the 2007 eruption compared to the main features of the 2002–2003 movement (α slide).

terrace down to −50 m, the bulging of the slope sector between 550–350 m a.s.l. due to strong horizontal displacements and the emplacement of the main lava flow that built a delta on the shoreline.

Both eruptions were associated to a dike intrusion that induced a relatively deep-seated failure at the slope top involving the same area with similar geometry. Fig. 12 clearly shows that the area lowered in 2007 coincides with the displaced and backward-tilted head of the initial deep-seated α slide of 2002. Conversely, the most striking difference between the effects of the two eruptions is the absence of a downward propagation of the instability in March 2007.

The comparison between the two events indicates that, as a consequence of different magma intrusion mechanisms, the slope evolution can follow either large destructive landsliding or large failure phenomena unaccompanied by a mass detachment. However, both eruptions were followed by depositional processes or slope erosion which tends to re-establish a more regular morphology which is distinctive of the SdF evolution in the absence of lava effusion.

7. Concluding remarks

The quantitative analysis we have carried out on the 2002–2003 and 2007 Stromboli eruptions, starting from data acquired through airborne remote sensing surveys, permitted the estimation of the lava volumes emplaced on the SdF slope and the corresponding average effusion rates. It also contributes to the investigation of the link between magma emission and slope instabilities.

Effusion rate data represents a key point for investigating the mechanisms that drive the effusive eruptions on Stromboli. Both eruptions were associated to a dike intrusion that produced a relatively deep seated failure which involved the same area at the slope top and produced morphological variations of relevant magnitude. The instabilities seem to be closely connected seeing as the displacements observed in 2007 may have been driven by sharp discontinuities within the deposit that formed in 2002–2003. The most striking difference between the effects of the two eruptions is the absence of down slope propagation during the 2007 instabilities.

The multi-temporal quantitative analysis of the SdF evolution during Stromboli's 2002–2003 eruption indicates that the slope can easily experience instabilities that may also involve highly destructive landslides which have significant tsunamogenic potential (Tommasi et al., 2003, 2005; Tinti et al., 2005). On the contrary, the observation and the analysis carried out on the 2007 eruption demonstrate that large deformation process does not necessarily produce mass failures.

The results presented in this work undoubtedly indicate that hazard assessment for the island of Stromboli should take into account the fact that a new magma intrusion could lead to further destabilisation of the slope, which may be more significant than the one recently observed because it will affect an already disarranged deposit and fractured and loosened crater area. The risks associated to a destructive slope evolution should be then assessed by means of systematic monitoring and appropriate modelling tools for predicting the slope's response to new stress variations.

Appendix A

The method adopted for evaluating the F2 flow volume integrates both the planimetric and topographic approaches. Three different

Table 5
Removed and filled areas, volumes and average thicknesses (volume divided per area) evaluated from DEM comparison for: the whole F2 flow (area *a*); the intersection between F2 and the landslide (area *b*); the landslide outside F2 limits (area *c*).

	Zone *a*			Zone *b*			Zone *c*		
	4 March	15–16 March	12 April*	4 March	15–16 March	12 April*	4 March	15–16 March	12 April*
A_{rem} (10^4 m^2)	0.79	0.54	0.00	0.61	0.50	0.00	0.89	0.00	0.00
V_{rem} (10^4 m^3)	1.36	0.70	–	1.22	0.67	–	1.83	–	–
T_{rem} (m)	1.73	1.29	–	2.00	1.34	–	2.07	–	–
A_{fill} (10^4 m^2)	3.40	11.65	17.50	0.52	2.26	2.95	0.60	0.00	0.00
V_{fill} (10^4 m^3)	18.34	138.84	264.70	0.85	12.59	37.07	1.48	–	–
T_{fill} (m)	5.40	11.91	15.12	1.63	5.56	12.58	2.46	–	–

*The corresponding values refers to the end of the eruption (2 April).

areas (Fig. 8) were defined on the zone affected by the F2 flow and the landslide: a) the whole F2 flow; b) the intersection between F2 and the landslide; and c) inside the landslide but outside the F2 limits.

The removed and filled volumes (Table 5) were evaluated by DEM comparison on the three areas, although the *c* evaluation has only been possible at 4 March because the lava flow at 15 March and 2 April covered the scar entirely. The average corresponding removed and filled thicknesses were then evaluated for the three areas (T^i_{rem}, T^i_{fill} where *i* corresponds to *a*, *b*, or *c* evaluation while *rem* or *fill* correspond to removed or filled).
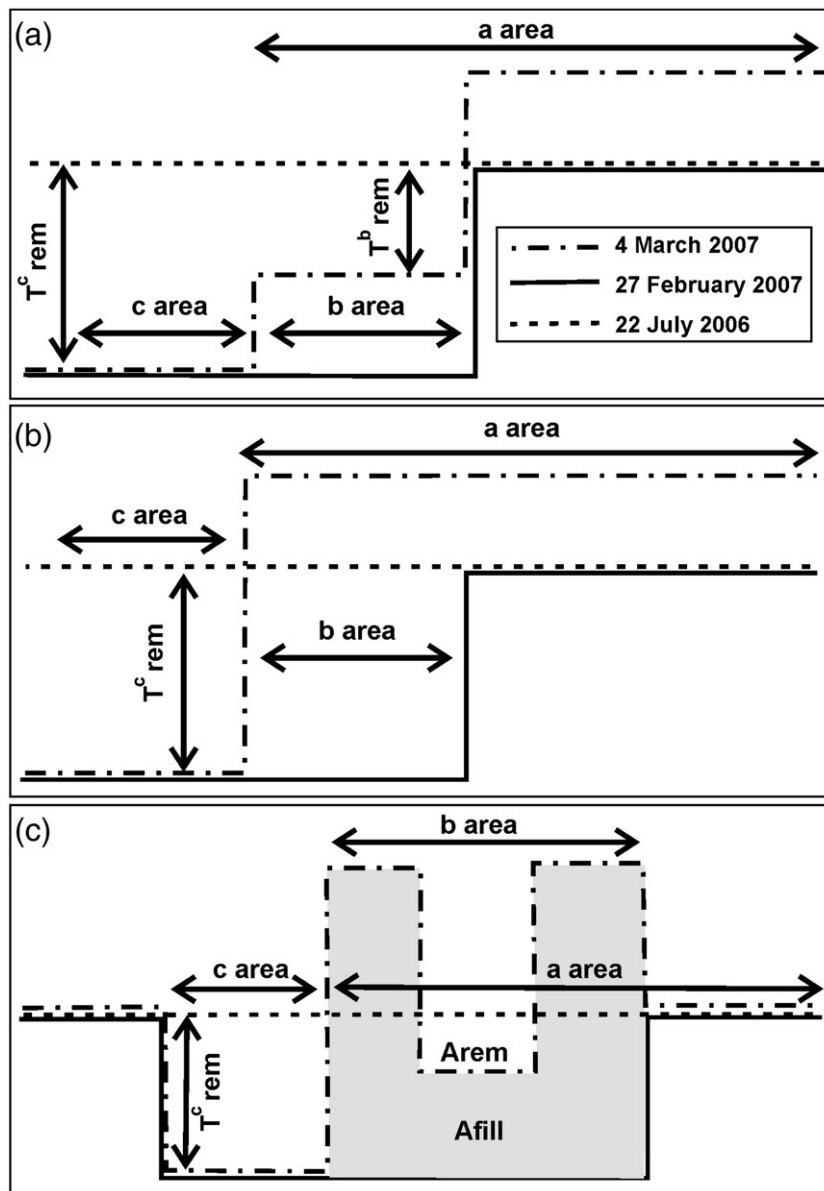
Fig. 13. Sketch supporting the estimate of the average lava thickness emplaced inside the landslide scar (b area in Fig. 8) for negative (a) and positive (b) residuals and of the volume removed by the landslide of 27 February 2007 (c). The legend in (a) refers to the three portions of the figure: dashed lines represent the pre-eruption topographic surface (July 2006); continuous lines represent the topographic surface at the beginning of the eruption (27 February 2007), that is soon after the landslide but before the opening of V2; dashed-dotted lines indicate the topographic surface at 4 March 2007, that is after the landslide and during V2 effusive activity.

Finally, the lava cumulated on the b area ($\tilde{V}$) was estimated by supposing that the average thickness of the scar left by the landslide was the same as in c (Fig. 13a and b). The equations for the average lava thickness are different for the b areas which have negative or positive residuals:

For the negative residual (T^b_{rem}), distributed above the area A^b_{rem} (Fig. 13a) the cumulated lava volume at 4 March (0.04×10^4 m^3) was evaluated as:

$$\tilde{V}^b_{rem} = A^b_{rem} \cdot \left(T^c_{rem} - T^b_{rem} \right)$$

For the positive residual (T^b_{fill}), distributed above the area A^b_{fill} (Fig. 13b), the cumulated lava volume at 4 March (1.25×10^4 m^3) was evaluated as:

$$\tilde{V}^b_{fill} = A^b_{fill} \cdot (T^c_{rem})$$

Thus the total volume of F2 at 4 March (Table 3) is

$$V^{F2}_{tot} = V^a_{fill} + \tilde{V}^b_{rem} + \tilde{V}^b_{fill}$$

The extension of the landslide did not change during the F2 emplacement, thus it is possible to estimate the total volume that it removed in the b and c areas (5.42×10^4 m^3) from the comparison between the 4 March 2007 and the pre-eruption DEMs and by supposing that the average thickness of the scar left by the landslide in b was the same as in c (Figs. 13c):

$$\tilde{V}_{land} = V^c_{rem} + \left(A^b_{rem} + A^b_{fill} + A^c_{fill} \right) \cdot T^c_{rem}$$

The total volume of F2 at 15–16 March (Table 3) is

$$V^{F2}_{tot} = V^a_{fill} + \tilde{V}_{land} - V^a_{rem}$$

The removed volume was subtracted because the landslide scar, at the 15–16 March, was not completely filled by the outpoured lava.

The total volume of F2 at 2 April (Table 3) is

$$V^{F2}_{tot} = V^a_{fill} + \tilde{V}_{land}$$

References

Andronico, D., Cristaldi, A., Taddeucci, J., 2007. Eruzione Stromboli 2007 L'evento parossistico del 15 marzo. http://www.ct.ingv.it/Report/RPTVSTRCEN20070315.pdf.

Baldi, P., Fabris, M., Marsella, M., Monticelli, R., 2005. Monitoring the morphological evolution of the Sciara del Fuoco during the 2002–2003 Stromboli eruption using multi-temporal. ISPRS J. Photogramm. Remote Sens. 59 (4), 199–211.

Baldi, P., Coltelli, M., Fabris, M., Marsella, M., Tommasi, P., 2008a. High precision photogrammetry for monitoring the evolution of the NW flank of Stromboli volcano during and after the 2002–2003 eruption. Bull. Volcanol. 70 (6), 703–715. doi:10.1007/s00445-007-0162-1.

Baldi, P., Bosman, A., Chiocci, F.L., Marsella, M., Romagnoli, C., Sonnessa, A., 2008b. Integrated Subaerial–Submarine Evolution of the Sciara del Fuoco After the 2002 Landslide. In: S. Calvari, S. Inguaggiato, G. Puglisi, M. Ripepe, M. Rosi (Editors), The Stromboli Volcano: An Integrated Study of the 2002–2003 Eruption (Geophysical monograph series, vol. 182), Washington, 171–182.

Calvari, S., Spampinato, L., Lodato, L., Harris, A.J.L., Patrick, M.R., Dehn, J., Burton, M.R., Andronico, D., 2005. Chronology and complex volcanic processes during the 2002–2003 flank eruption at Stromboli volcano (Italy) reconstructed from direct observations and surveys with a handheld thermal camera. J. Geophys. Res. 110 (B02201). doi:10.1029/2004JB003129.

Coltelli, M., Proietti, C., Branca, S., Marsella, M., Andronico, D., Lodato, L., 2007. Analysis of the 2001 lava flow eruption of Mt. Etna from three-dimensional mapping. J. Geophys. Res. 112 (F02029). doi:10.1029/2006JF000598.

Cristaldi, A., 2007. Rapporto settimanale sull'attività eruttiva dello Stromboli ripresa dalle telecamere di sorveglianza. http://www.ct.ingv.it/Report/WKRVGALT20080305.pdf.

Graziani, A., Tommasi, P., Verrucci, L., 2007. Effetti dell'intrusione superficiale del magma sulla stabilità della Sciara del Fuoco (Stromboli). Proc. Incontro Annuale dei Ricercatori di Geotecnica — IARG 2007, Salerno, Italy. 4 pp.

Itasca, 2006. FLAC 3D User's Manuals. Itasca Consulting Group Inc., Minneapolis.

Kovari, K., Fritz, P., 1984. Recent developments in the analysis and monitoring of rock slopes. Proc. 4th Int. Symp. on Landslides, Toronto, Canada. 17 pp.

Maramai, A., Graziani, L., Tinti, S., 2005. Tsunamis in the Aeolian Islands (southern Italy): a review. Mar. Geol. 215, 11–21.

Marsella, M., Coltelli, M., Proietti, C., Branca, S., Monticelli, R., 2008. 2002–2003 lava flow eruption of Stromboli: a contribution to understanding lava discharge mechanism using periodic digital photogrammetry surveys. In: Calvari, S., Inguaggiato, S., Puglisi, G., Ripepe, M., Rosi, M. (Eds.), The Stromboli Volcano: An Integrated Study of the 2002–2003 Eruption. . Geophysical monograph series, vol. 182. AGU, Washington, pp. 229–246.

Moore, J.G., Phillips, R.L., Grigg, R.W., Peterson, D.W., Swanson, D.A., 1973. Flow of lava into the sea, 1969–1971, Kilauea Volcano, Hawaii. Geol. Soc. Amer. Bull. 84 (2), 537–546.

Neri, M., Lanzafame, G., Acocella, V., 2008. Dyke emplacement and related hazard in volcanoes with sector collapse: the 2007 Stromboli (Italy) eruption. J. Geol. Soc. 165, 883–886. doi:10.1144/0016-76492008-002.

Puglisi, G., Bonaccorso, A., Mattia, M., Aloisi, M., Bonforte, A., Campisi, O., Cantarero, M., Falzone, G., Pugliesi, B., Rossi, M., 2005. New integrated geodetic monitoring system at Stromboli volcano (Italy). Eng. Geol. 79, 13–31.

Ripepe, M., Marchetti, E., Ulivieri, G., Harris, A., Dehn, J., Burton, M., Caltabiano, T., Salerno, G., 2005. Effusive to explosive transition during the 2003 eruption of Stromboli volcano. Geology 33 (5), 341–344.

Rittmann, A., 1931. Der ausbruch des Stromboli am 11 September 1930. Zeitschrift für vulkanologie 14, 47–77.

Rosi, M., Bertagnini, A., Harris, A.J.L., Pioli, L., Pistolesi, M., Ripepe, M., 2006. A case history of paroxysmal explosion at Stromboli: timing and dynamics of the April 5, 2003 event. Earth Planet. Sci. Lett. 24 (3–4), 594–606.

Stevens, N.F., Wadge, G., Murray, J.B., 1999. Lava flow volume and morphology from digitised contour maps: a case study at Mount Etna, Sicily. Geomorphology 28, 251–261.

Tinti, S., Manucci, A., Pagnoni, G., Armigliato, A., Zaniboni, F., 2005. The 30 December 2002 landslide-induced tsunamis in Stromboli: sequence of the events reconstructed from the eyewitness accounts. Nat. Haz. Earth Syst. Sci. 5, 763–775.

Tommasi, P., Chiocci, F.L., Coltelli, M., Marsella, M., Pompilio, M., 2003. Analysis of the first data on the instability phenomena associated to the 2002–03 Stromboli volcano lava flow eruption. Proceedings of Int. Symposium Flows 2003, Sorrento, Italy. 10 pp.

Tommasi, P., Baldi, P., Chiocci, F.L., Coltelli, M., Marsella, M., Pompilio, M., Romagnoli, C., 2005. The landslide sequence induced by the 2002 eruption at Stromboli volcano. In: Sassa, K., Fukuoka, H., Wang, F.W., Wang, G. (Eds.), Landslide — Risk Analysis and Sustainable Disaster Management. Springer Verlag, Berlin, pp. 251–258.

Tommasi, P., Boldini, D., Cignitti, F., Graziani, A., Lombardi, A., Rotonda, T., 2007. Geomechanical analysis of the instability phenomena at Stromboli Volcano. In: Eberardt, E., Stead, D. (Eds.), I Canadian — U.S. Rock Mechanics Symposium, Vancouver, vol. 2, pp. 933–941.